Title: Thermo-mechanical pressurization of experimental faults in cohesive rocks during seismic slip

Authors: Violay, M.[1,2*], Di Toro, G.[3,4], Nielsen, S.[5], Spagnuolo, E.[6], Burg, J.P.[1]

Affiliations:

[1] ETH D-ERDW, Sonnegstrasse, 5 CH-8092, Zürich, Switzerland

[2] EPFL-ENAC, LEMR, Station 18 CH-1015, Lausanne, Switzerland

[3] Dipartimento di Geoscienze, Università degli Studi di Padova, Via G. Gradenigo 6, 35131, Padua, Italy

[4] School of Earth, Atmospheric & Environmental Sciences, University of Manchester, Oxford Road, Manchester M13 9PL, UK

[5] Earth Sciences Department, University of Durham, South Road, Durham DH13LE, UK

[6] Istituto Nazionale di Geofisica e Vulcanologia, Via di Vigna Murata 605, 00143, Rome, Italy

**Correspondence to: marie.violay@erdw.ethz.ch*

Highlights:

High velocity friction experiments on cohesive rocks under undrained conditions

Experimental evidence of thermo-mechanical pressurization (TMP)

TMP weakening of cohesive rocks is negligible during earthquakes

Keywords:

Friction, earthquakes, fluids, thermo-mechanical pressurization, basalt, marble

Abstract:

Earthquakesoccur because fault friction weakens with increasing slip and slip rates.Since the slipping zones of faults are often fluid-saturated, thermo-mechanical pressurization of pore fluids has been invoked as a mechanismresponsible for frictional dynamic weakening, but experimental evidence is lacking.We performed friction experiments(normal stress 25 MPa, maximal slip-rate~3 ms^{-1})oncohesive basalt and marbleunder(1)room-humidityand (2)immersed in liquid water(drained and undrained) conditions. In both rocks and independently of the presence of fluids, upto 80% of frictional weakening wasmeasured in the first 5 cm of slip. Modest pressurization-related weakening appears only at later stages of slip. Thermo-mechanical pressurization weakening of cohesive rocks can be negligible during earthquakes, due to the triggering of more efficient fault lubrication mechanisms (flash heating, frictional melting, etc.).

Introduction

During earthquakes,few millimeters thick slip zones within fluid-saturated, cohesiveornon-cohesive rocksare shearedup to several meters (80 m for the Tohoku 2011 Mw 9.0 earthquake, **Fujiwara et al., 2011**)at slip rates of meters per second and under normal stressesup to hundreds of MPa (**Sibson, 1973; Rice, 2006**). The frictional power per unit area (product of the slip rate per frictional shear stress, in the range of 1-100 MW m^{-2}) dissipated in the slipping zone is exchanged into heat and rock fragmentation (**Sibson, 1980**). The large power dissipated during slip triggers several mechano-chemical processeswhich mayinducefrictional weakening (**Di Toro et al., 2011; Goldsby and Tullis, 2011; Reches and Lockner, 2010**). Thermo-mechanical pressurization (TMP) of pore fluids trapped in slipping zones is one of the possible processes responsible for fault dynamic weakening(**Sibson, 1973; Rice,1992; 2006;Lachenbruch, 1980;Brantut et al., 2010;Bizzari and Cocco, 2006; Segall and Rice, 2008; Wibberley and Shimamoto, 2005**). Given the widespread presence of fluids in natural slipping zones, TMP has been thoroughlyinvestigated from a theoreticalpoint of view. TMP models are based on two competing processes: fluid and rock expansion in response to shear heating and the fluid storage capacity of the rock(**Rice, 2006;Segall and Rice, 2008; Platt et al., 2014**).

Several experimental studies were carried on to investigate TMP (**Mizoguchi et al., 2009; Brantut et al., 2011; Ferri et al., 2010; 2011; De Paola et al., 2011; Mitchell et al., 2015; Faulkner et al., 2011; Ujiie et al., 2011; 2013)**. Experiments approached seismic deformation conditions by imposing slip rates (*V*) of ~1 ms^{-1}, slip (δ) up to tens of meters, and effective normal stresses (σ_n^{eff})of tens of MPa) on clay-, calcite- and dolomite-rich gouges under room-humidity and wet conditions. The large weakening (up to 80-90% of friction drop at 1 ms^{-1}) measured was(1) in the case of the room-humidity experiments, in part (< 20%) attributed to thermochemical pressurization associated to the breakdown of clays and releaseof H_2O (**Brantut et al., 2011; Ferri et al., 2010**) or to the breakdown of calcite and dolomite and release of CO_2 (**De Paola et al., 2011; Mitchell et al., 2015**)and, (2) in the case of the wet experiments on clay-rich gouges,to thermal pressurization (**Faulkner et al., 2011;Ferri et al., 2010;Ujiie et al., 2011; 2013**). However, technical issues related to fluid and gouge confinement impededto measure the pore fluid pressure in the sample chamber. Recently, we installed on the rotary shear machine SHIVA(Slow-to-High-Velocity-Apparatus, INGV Rome, **Suppl. Material S1**) an on-purpose designed pressure-vessel which allows shearing cohesive rocks immersed in fluids and to measure the pore fluid pressureduring the experiments (**Violay et al., 2013**). Previous experiments were performed under drained conditions on Carrara marbles and gabbros (**Violay et al., 2013; 2014**). Here we report novel results obtained by shearing basalts and Carrara marbles under undrained conditions. Though the actual experimental configuration does not allow us to shear saturated gouges, the results for cohesive rocks are intriguing: the contribution of TMP during shearing of cohesive rocks at seismic slip rates is negligible compared to the contribution from other weakening mechanisms.

Material and methods

To investigate seismic slip in the presence of pore fluids, 33friction experiments (**Table1)** were conducted at room temperature on hollow cylinders (50/30 mm external/internal diameter) of Etna basalt(Electron Micro-Probe Analysis reported in **Table2**) and Carrara marble (99.9% calcite, X-Ray Diffraction and X-Ray Fluorescence analysis, **Violay et al., 2013**). Samples were jacketed with aluminum rings, sealed with epoxy to prevent fluid leaks and inserted in the fluid pressure vessel (**Nielsen et al., 2012**; **Suppl. Material S1**). The description of SHIVA (**Di Toro et al., 2010; Niemeijer et al., 2011**) and of the experimental configuration which allowed us to perform experiments with pressurized fluids can be found in **Suppl. Material S1**. The main difference with respect to previous studies conducted with fluids (**Violay et al., 2013; 2014**) was the disposition of the closed valves, which allowed us to impose undrained conditions in the experiments (see **Suppl. Material S1**for full description**)**. Experiments were performed (1) under room-humidity conditions and immersed in water and under either (2) drained conditions (the specimen is saturated and continuously connected to the water reservoir, (**Paterson and Wong, 2005)**, resulting in constant fluid pressure and preventing fluid pressurization), or (3) undrained conditions (the specimen was first saturated and then isolated from the water reservoir: fluid pressurization was induced by reduction in pore volume,(**Paterson and Wong, 2005)**, and by increase in fluid volume due to thermal expansion during shearing).A K-Type thermocouple was inserted at about 3 mm from the slip surface of the sample to measure the temperature evolution of the fluid during the experiments. The thermocouple was installed in the "stationary side" (i.e., normal stress loading column) of SHIVA.

Experiments were performed by spinning two rock cylinders at accelerations of 7.8 ms^{-2}, V= 3 ms^{-1}, 4m<δ<8m, normal stress (σ_n) from 15 to 35 MPa and initial fluid pressure P_{ini}=5 MPa(**Violay et al.,2013; 2014**).Mechanical data (axial load, torque, slip, angular rotation) were acquired at a frequency up to 25 kHz. δ, $V$and shear stress (τ) were determined using methods outlined in**Di Toro et al.** (2010), **Niemeijer et al.,** (2011) and **Tsutsumi and Shimamoto** (1997).Thetwo rock-types were selected because are quite common crustal rocks and for their relatively low porosity (<5%) and low permeability (<$10^{-17}$$m^2$)(e.g., **Vinciguerra et al., 2005**).The slip zonesof experiments conducted on basaltscould be recovered because the two rock cylinders were welded by glass due to the solidification of the frictional melt produced during shearing. Themicrostructures wereinvestigated with an optical microscope andelectron probe micro-analyzer (JEOL, JXA-8200 at ETH, Zurich). The chemical compositions of grains and glasses weredetermined on carbon-coated, polished thin sections using an Electron Probe Micro-Analyzer (EPMA) JEOL, JXA-8200(ETH, Zurich) with a focused beam about 1 μm in diameter under accelerating voltage of 15 kV and current 15 nA.The slipping zones of experiments conducted on Carrara marble could not be recovered *in-situ*(only few dispersed remnants were found) because they consisted of non-cohesive materialthat was flushed away during the ejection of the fluid from the vessel after the experiment.

Results

Mechanical data

Experiments performed under identical ambient and deformation conditions resulted in systematically reproducible mechanical data for both Etna basalt and Carrara marble (**Figs.1-4**). We present below the measurements of the friction coefficient ($\mu = \tau / \sigma_n^{eff}$or Terzaghi's principle for $\sigma_n^{eff} = \sigma_n - \alpha P_f$ withα =1, incorporating instantaneous σ_n and P_f) for comparison of data obtained at different initial effective normal stresses and the measurements of theshear stress for comparison of data obtained at a given imposed initial effective normal stress (all mechanical data are summarized in **Table 1**).

For Etna basalt, the coefficient of friction decayed almost exponentiallyfrom apeak value μ_{p}=0.59±0.08at about the initiation of slip (i.e., 0.64±0.05 for room humidity conditions, 0.58±0.05 for drained and 0.53±0.07 for undrained conditions) to a steady-state value μ_{ss}that decreased with increasing effective normal stress (**Figs. 1 and4**).The $\mu_{\text{ss}}$was determined from the average valueof the normal stress, pore fluid pressure and shear stress between 4.5 and 5.5 meters slip, except for experiment S921 where μ_{ss} was determined between 2.5 and 3.5 meters slip.Theinitial decay of the friction coefficient (and thus of the shear stress)was quite similar independently of the ambient conditions (**Fig. 3**). At σ_n^{eff}= 20 MPa, the residual friction coefficient after 5 cm of slip ranged from$\mu_{\text{r_5cm}}$= 0.20-0.25 for the room humidity (s485 and s541), to $\mu_{\text{r\_5cm}}$ = 0.26-0.28 for the drained (s921 and s926) and to $\mu_{\text{r\_5cm}}$ = 0.22-0.24 for the undrained (s922, s925, s927 and s933) experiments (**Table 1**).The $\mu_{\text{r_5cm}}$corresponded to a percentage of friction drop with respect to μ_{p}(or %$\Delta\mu$ = 100 ($\mu_{\text{r\_5cm}}$ -μ_{ss})/(μ_{p}- μ_{ss})) ranging from80.2% (s485, room humidity conditions), to 56.4% (s921, drained conditions)**(Fig.4, and Table 1)**. Given the larger μ_{p} in the room humidity experiments, the drop in percentage of the friction coefficient in the first 5 cm of slip was slightly larger in room humidity conditions (73.06±5.24%) than in both drained (67.96±8.36%) and undrained (68.35±3.65%) conditions (**Fig. 4**).

Instead, the steady-state shear stress (τ_{ss}) was about 20% lower under undrained than under drained and room-humidity conditions, for similar V, δ, and $\sigma_{\text{n}}^{\text{eff}}$(**Figs. 2, 3, Suppl. Material S2**). For instance, at σ_n^{eff}= 20 MPa, the coefficient of friction decayed from a peak value μ_{p} = 0.55∓0.07 (corresponding to a shear stress of 11±1.4 MPa) towards a steady-state value μ_{ss} = 0.11∓0.01 (shear stress of 2.2±0.2 MPa) under room-humidity conditions, μ_{ss} =

0.11∓0.01 (shear stress of 2.2±0.2 MPa) under drained conditions and μ_{ss} = 0.09∓0.01 (shear stress of 1.8±0.2 MPa) under undrained conditions (**Table 1; Fig. 2**).Under undrained conditions, an overpressure *dP*(such that $P_f = P_{ini} + dP$) was measured with increasing slip (**Fig.2A**) following a power lawbest fitted by $dP = 8.4\ (\mp 0.6)\ \delta^{0.2(\mp 0.07)}$ [MPa] (for σ_n= 25 MPa, V=3 ms^{-1} P_{ini}=5 MPa).Overpressure *dP* decreased immediately of ~60% after the slip stopped (**Fig.2A).** Conversely, P_f and σ_n did not vary under drained conditions (**Fig.2A**). Sample shortening rate was constant and almost negligible during the first fivecentimeters of slipfor both drained and undrained conditions (**Fig.3B**). At sliplonger than 5 cm, the shortening rate was ~0.170mm/m and ~0.089mm/m for drained and undrained conditions, respectively**(Fig.1, Table1).**

For Carrara marble, the friction coefficient evolved fromμ_p= 0.60±0.07 to μ_{ss}= 0.04±0.02**(Table1)**. Contrary to Etna basalt, $\tau_{ss}$and shortening rate were almost negligible andsimilar (~0.0001 mm/m) under room humidity, drained and undrained conditions, even if a small pore fluid overpressure (*dP* ~1 MPa) was measured after several meters of slip under undrained conditions(**Fig.2B**). The μ_{r_5cm} was larger (and similar) for both undrained (68.96±1.79%) and drained (70.44±2.58%) conditions, than under room humidity (49.85±4.39%) conditions (**Table1; Fig. 4D**).

Temperature measurement

The maximum temperature measured by the thermocouple immersed in the fluid was 35 ºC for experiment s929 performed at normal stress of 25 MPa, initial fluid pressure of 5 MPa, target slip rate of 3 ms^{-1}and total slip of 6 m**(Fig. 5).** The thermocouple measured the temperature evolution with time of the water in the pressure vessel due to the frictional heat generated and diffused from the slip surface. Because of heat diffusion in water, the thermal perturbation was detected with some delay with respect to the initiation of the experiment. This renders the determination of the temperature of the sliding surface a quite complicated task.

Microstructures

After the experimentsand irrespective of the ambient conditions, in Etna basalt, a continuous 100-200 μm thick layer of glassy-like materialseparated the rock cylinders**(Fig.6)**. Under the optical microscope, the layer was homogeneous and brown in color in parallel-polarized light, and extinct in cross-polarized light, suggesting that the layer was made of solidified friction melt (i.e., glass). This interpretation is consistent with the visible extrusion of drops of melt during experiments performed at room-humidity conditions, and with the presence, in all the experiments, of a lump of glassy-like material preserved in the inner hole of the hollow cylinders. The electron microprobe analysis showed that, independently of the environmental conditions, in all the experiments where steady-state friction was achieved, the glass had a chemical composition almost identical to the bulk composition of the initial Etna Basalt **(Table2).**From image analysis of FE-SEM microphotographs, the glassy-like layer of experiments performed under room-humidity contained < 1% in volume of vesicles and ~16 ± 5% in volume of lithic clasts (< 10 μm in size); instead, in the case of experiments performed in the presence of fluids, the glassy-like layer contained 3±2% in volume of vesicles and ~9±3 % in volume of lithic clasts (< 10 μm in size) in both drained and undrained conditions**(Fig.6).**

For Carrara marble, in the case of the room-humidity experiments performed at σ_n^{eff}= 20 MPa, δ=4÷7 m and $V = 3\ ms^{-1}$ s, the wall rocks were separated by ~100 μm thick continuous slip zone composed of fine-grained (< 50 nm in size) non-cohesive material (see Fig. 5 in**Violay et al., 2013**).In the case of the drained and undrained experiments, the compacted gouge layerswere not investigated because were not found on the slip zone.

Discussion

In the two rock types under both room-humidity and drained conditions,$\mu_p$andμ_{ss}were consistent with those previously measured in basaltic**(Violay et al., 2014)**and carbonate-bearing rocks**(Han et al., 2007; 2010; Violay et al., 2013)**.Comparison between room-humidity anddrainedexperiments showsthat the presence of waterhad almost no effect on $\mu_p$andμ_{ss}(**Figs.2-4***)***(Violay et al., 2014).**However, for Etna basalt, experiments performed under undrained conditions (**Fig.2**)had about 20% reduction ofτ_{ss}compared to room-humidity and drained experiments. Moreover, the fluid pressure increased with slipunder undrained conditions, but was constant under drained conditions (**Fig.2**).This is furthermore supported by a temperature increase of 35ºC measured by the thermocouple immersed in the fluid inthe case of undrained experiments (**Fig.5**), and < 5ºC in drained experiments (for σ_n^{eff}= 20 MPa, δ= 7 m and V = 3 ms^{-1}). The undrained thermal pressurization coefficient defined as the pore pressure increase for a unit temperature increase ranges from 0.01 MPa/°C to 0.1 MPa/°C**(Ghabezloo and Sulem, 2009).**An increase in bulk temperature of 35ºC of the fluid results in an increase in pore pressure of 0.35–3.5 MPa. We interpret the reduction of $\tau_{ss}$to be the result of TMPwithin the slipping zone. Themeasured shear stress reduction is consistent with the melt lubrication model by **Nielsen et al. (2008)**according to which the rate of extrusion of friction melt from the slipping zone is regulated by the difference between the viscous pressure of the meltand the normal stress acting on the fault. Although the Terzaghi'sprinciplecannot be appliedunder melt-lubricated conditions, we can draw a parallel about the role of the effective normal stress: the increase in fluid pore pressure in theslipping zone limits the melt extrusion rate from the slipping zone in the same way as the decrease of the normalstress acting on the fault.In both cases, the bulk result is the reduction of the viscous shear stress.This is confirmed by the lower sample shortening rate under undrained (e.g., 0.089 mm/m) than drained (0.17 mm/m) conditions**(Fig. 2A and Table 1)**.Under undrained conditions, after the slipstopped,part of the pressurization *dP*in excess of P_{ini}gradually decreased**(Fig. 2A)**. Thisindicates that *thermal*pressurization (due to water thermal expansion during frictional heating) wasdropping upon cooling of the water (by conduction through the vessel metal).A residual *mechanical*pressurization endured after cooling, due to the permanent volume reduction in connection to sample shortening.

In spite of the evidence of a measurable TMP, we question whether it is an efficient fault weakening mechanism during seismic slip, in particular in the presence of more rapid and effective alternative mechanisms.Under undrained conditions, fluid overpressures of ~1 MPa and 0.05 MPa weremeasured after 5 cm of slipfor Etna basalt and Carrara marble,respectively (**Figs. 2A-B; 3A**). The initial overpressure (*dP*) was associated to a relative (dP*100/τ_p)apparent shear stress drop of maximum10% for σ_n^{eff}=20 MPa in Etna basalt (squared dots in **Fig.4**), and no shear stress drop in Carrara Marble. Since the shear stress drop was65-80% after5 cm of slip for both lithologies, more efficient lubricating mechanisms must have been activatedat the initiation of slip and at steady-state, (note that, based on previous observations **(Violay et al., 2013),** cavitation and Elasto-dynamic lubrications are excluded in the interpretation of weakening in our experiments).In both rock-types, at the initiation of slip, the negligible contribution of TMP to the large frictional weakening of the experimental fault is further supported by the absence of variations in either normal stress or shortening (i.e. no evidence of dilatation)(**Fig.3B**). Though TMP is negligible in the initial weakening phase, it may affect later stages of slip, thus reducing the residual strength (dynamic sliding value after weakening). Indeed this may have consequences on (1) the dynamic stress drop during rupture and (2) a slight increase in the equivalent fracture energy for frictional weakening, i.e., the area below the weakening curve and above the minimum sliding friction (Abercrombie and Rice, 2005).

However, at steady-state, the ineffectiveness of TMP is demonstrated by **1)**the occurrence of solidified friction melts, which cover the surface of Etna Basalt cylindersindependently of the presence or absence of fluids. The experimental and microstructuralobservations suggest that the dominant weakening mechanism was flash heating causing melting at the asperity contacts at the initiation of slipand frictionalmelt lubrication at steady-state**(Goldsby and Tullis, 2011, Brown and Fialko, 2012, Violay et al., 2014)** and**2)**the occurrence of ultrafine-grained material in water for Carrara marble experiments, independently of the hydraulic conditions. The experimental and microanalytical observations suggest that the dominant weakening mechanism in Carrara marble was probablyfash heating of the asperitiesat the initiation of sliding **(Violay et al., 2013, Spagnuolo et al., subm.)**or a grain-size(possibly water-enhanced) dependent process (super-plasticity) at steady-state**(Verberne et al., 2014; Green et al., 2015; De Paola et al., subm.,).**

At the initiation of sliding, the apparently small contribution of measured TMP to fault weakening under drained and undrained conditions might be due in part to the experimental configuration. Indeed, at short time intervals, heating affects only the water volume trapped in the slipping zone (Vol_s~2 $10^{-7}m^3$, given the average thickness of ~0.16 mm induced by sample roughness over the 12.5 10^{-4} m^2 of slipping area), which is small compared to the fluid volume in the vessel (Vol_v~5 10^{-6} m^3). For reasonable fault-parallel permeability the water on the slipping zone and in the vessel are connected and pressure is at equilibrium. Then the volume expansion of heated slip-zone water:

$$dVol_{exp} = \lambda \Delta T Vol_s \qquad \text{Eq. 1}$$

is accommodated by the total water volume (λ being the water coefficient of thermal expansion). Assuming roughly constant λ, K (water incompressibility) and total available volume Vol_s+Vol_v (i.e., neglecting volume changes due to compliance of the vessel or of rocks on natural faults), we obtain aupperbound pressurization reached during fault slip:

$$dP = K\, dVol_{exp}/(Vol_s+Vol_v) = K\, \lambda\, \Delta T\, Vol_s/(Vol_s+Vol_v) \qquad \text{Eq. 2}$$

On actual faults the volume of connected water (equivalent to Vol_v) per unit fault surface may be smaller than in the experiment, a condition which is readily extrapolated by reducing Vol_v in expression (1). In order to estimate the maximum contribution of TMP to frictional weakening, we assume VolV close to zero. The upper bound is thus obtained assuming that (1) the heat produced by frictional sliding is entirely dissipated in a small water volume trapped in the slipping zone (Vols), (2) volume changes due to compliance of the vessel or of rocks on natural faults are negligible and (3) the buffering effect of thermal expansion of water by the connected volume is reduced to zero.

Using λ=207 10^{-6} ºC^{-1}, K=2.1 GPa**(Waples and Waples, 2004),** Vol_v=0 and an estimated temperature increase of 20ºC after a slip of 0.1 mwe obtain a pressurization of ~1.1 MPa at most.Note that the bulk temperature increase in the slipping zone (for $\tau(t) = \mu(t)\,(\sigma_n - P_f)$) was estimated using the heat rate production and solving the 1D diffusion problem (Carslaw and Jaeger, 1959) such that:

$$T(t) = \frac{1}{\rho \cdot Cp \cdot \sqrt{\kappa\pi}} \cdot \int_0^t \frac{1}{2} \cdot \frac{\tau(t') \cdot V(t')}{\sqrt{t-t'}}\, dt \qquad \text{Eq. 3}$$

(where thermal capacity Cp = 880 J kg^{-1}K^{-1} and 116 J kg^{-1} K^{-1}respectively for calcite and basalt samples, density ρ = 2700 kg m^{-3}and 2900 kg m^{-3}respectively for calcite and basalt sample and thermal diffusivity κ = 1.48 10^{-6} m^2 s^{-1}0.21m^2 s^{-1}respectively for calcite and basalt sampleand t is the time need to slip between 0 and 100 mm (**Eppelbaum et al.,2014;Hanley et al., 1978; Waples and Waples, 2004;** for further details see **Violay et al., 2013).**From equations 2 and 3, the thermal pressurizationof 1.1 MPa would induce a friction drop of about 15% from peak stress; but such drop was already achieved before 0.01 m of slip, even in drained or room-humidity experiments (**Fig. 3**). As a consequence, upon extrapolation to conditions where the water volume surrounding the fault is negligible, thermal pressurization is still rather less efficient than other weakening mechanisms (e.g., flash weakening and heating of asperities) and would add a further relative weakening to an already lubricated fault.The contribution from thermal pressurization will decrease with increasing fluid connectivity and can bequantified as follows. From Eq. 2, the fluid volume expansion dVol_{exp} due to the temperature increase results in an increase inpore fluid pressure:

$$P_f = P_{ini} + K \frac{\lambda\, \Delta \mathrm{T}\, Vol_s}{Vol_v + Vol_s} \qquad \text{Eq. 4}$$

The weakening due to water pressurization$w_p$increases with P_f:

$$w_p = \frac{\sigma_n - P_f}{\sigma_n - P_{ini}} \text{ Eq. 5}$$

and is related to the connected fluid volume (in m^3) per unit fault surface in m^2. Value of $w_p = 1$ correspond to no contribution to weakening from pressurized fluids (i.e., $P_f = P_{ini}$). From **Fig. 7**, the maximum effect of pressurization is a drop to 40% for connected volumes of less than a cubic centimeter per unit fault area (corresponding to 10^{-6} m). For values above 1 literof connected water per unit fault area (corresponding to a water layer of average thickness 1 mm) the pressurization effect is buffered and negligible.

Conclusions

We conclude that even extremely thin (< 100 μm) and low permeability (<10^{-17} m^2 slipping zones,may lead to a relatively unimportant TMP of pore fluids during seismic slip. These observations applyto slip surfaces within cohesive rocks where strain localization is instantaneous resulting in rapid temperature increase of the slipping zone leading to the activation of other weakening mechanisms**(Rice, 2006, Goldsby and Tullis, 2011, Di Toro et al., 2010).**In the case of non-cohesive rocks (gouges), before it localizes, strain is distributed within the gouge layer**(Beeler et al., 1996, Marone et al., 1990, Smith et al., 2015)**. These resultsin a gradual temperature increase during slip and TMP of pore fluids might still be an efficient fault weakening mechanism.

References

Abercrombie and Rice, 2005, Can observations of earthquake scaling constrain slip weakening? Geophys. J. Int. 162, pp. 406–424, doi: 10.1111/j.1365-246X.2005.02579.x

Beeler N.M., et al., 1996. Frictionalbehavior of large displacement experimental faults.J. Geophys. Res., 101, 8697-8715

Bizzari, A. Cocco, M, 2006. A thermal pressurization model for the spontaneous dynamic rupture propagation on a three-dimensional fault: 1. Methodological approach. J. Geophys. Res., 111, B05303

Brantut, N. et al., 2010. Thermochemical pressurization of faults during coseismic slip, J. Geophys. Res., 115, B05314

Brown K. M., Fialko Y., 2012. Melt welt' mechanism of extreme weakening of gabbro at seismic slip rates. Nature, 488, 638-41

De Paola, N., Hirose, T. Mitchell, G. Di Toro, C. Viti, and T. Shimamoto (2011), Fault lubrication and earthquake propagation in thermally unstable rocks, Geology, 39, 35–38.

De Paola, N., Holdsworth, R.E., Viti, C., Collettini, C., Bullock, R. Can grain size sensitive flow lubricate faults during the initial stages of earthquake propagation, submitted to Earth and Planetary Science Letters.

Di Toro G. et al., 2011. Fault lubrication during earthquakes. Nature, 471, 494-498.

Di Toro G. et al., 2010. From field geology to earthquake simulation: a new state-of-the-art tool to investigate rock friction during the seismic cycle (SHIVA). RendicontiLincei, 21, 95–114

EppelbaumL. et al., Applied Geothermics, Lecture Notes in Earth System Sciences, DOI: 10.1007/978-3-642-34023-9_2Springer-Verlag Berlin Heidelberg 2014

Faulkner D.R., Mitchell T.M., Behnsen J., Hirose T., Shimamoto T. 2011 Stuck in the mud? Earthquake nucleation and propagation through accretionary forearcs Geophysical Research Letters, 38.

Ferri F., et al., 2010. Evidences of thermal pressurization in high velocity friction experiments on smectite-rich gouges Terra Nova, 22, 347–353

Fujiwara T. et al., 2011. The 2011 Tohoku-Oki Earthquake: Displacement Reaching the Trench Axis. Science, 334, 1240-1240

Ghabezloo S., Sulem J., 2009.Temperature induced pore fluid pressurization in geomaterials RockMech Rock Eng, 29-43

Genevois, R., &Ghirotti M. 2005. The 1963 Vaiont landslide, G. Geol. Appl., 1, 41–53

Goldsby D.L., Tullis T.E. 2011. Flash heating leads to low frictional strength of crustal rocks at earthquake slip rates. Science, 334, 216-218.

Green, H.W., Shi, F., Bozhilov, K., Xia, G., Reches, Z., 2015. Phase transformation and nanometric flow cause extreme weakening during fault slip. Nature Geoscience, DOI:10.1038/NGEO02436

Han R. Hirose, T., Shimamoto T., 2010. Strong velocity weakening and powder lubrication of simulated carbonate faults at seismic slip rates. J. Geophys. Res. 115, B03412

Han R., et al., 2007. Ultralow friction of carbonate faults caused by thermal decomposition, Science. 316, 878–881

Hanley, E.J., Dewitt, D.P., Roy, R.F., 1978. The thermal diffusivity of eight well characterized rocks for the temperature range 300–1000 K. Eng. Geol. 12, 31–47.

Hirose T, Shimamoto T., 2005. Growth of molten zone as a mechanism of slip weakening of simulated faults in gabbro during frictional melting. J. Geophys. Res., 110, B05202

Lachenbruch, A.H., 1980. Frictional heating, fluid pressure, and the resistance to fault motion. J. Geophys. Res., 85, 6097–6122.

Marone C., Raleigh C.B., Scholz C.H., 1990. Frictional behavior and constitutive modeling of simulated fault gouge. J. Geophys. Res., 95, 7007-7025

Mitchell T.M., Smith S.A.F., Anders M.H., Di Toro G., Nielsen S., Cavallo A., Beard A.D. 2015. Catastrophic emplacement of giant landslides aided by thermal decomposition: Heart Mountain, Wyoming Earth Planet. Sci. Lett., 411, 199–207.

Mizoguchi, K., Hirose, T., Shimamoto, T. and Fukuyama, E., 2009. High-velocity frictional behavior and microstructure evolution of fault gouge obtained from Nojima fault, southwest Japan. Tectonophysics, 471, 285–296

Nielsen, S. et al., 2008. Frictional melt and seismic slip. J. Geophys. Res., 113, B01308.

Niemeijer, A. et al., 2011. Frictional melting of gabbro under extreme experimental conditions of normal stress, acceleration, and sliding velocity. J. Geophys. Res., 116, B07404.

Paterson, M. S., Wong T.-F., (2005). The brittle field, Second ed., 347, Springer Verlag, Berlin, New York.

Platt J. D., Rudnicki J. W., Rice J. R., 2014. Stability and Localization of Rapid Shear in Fluid-Saturated Fault Gouge, 2. Localized zone width and strength evolution, J. Geophys. Res., 119, 4334-4359

Reches, Z, Lockner D.A., Fault weakening and earthquake instability by powder lubrication. Nature, 467, 452-455

Rice J.R., 2006. Heating and weakening of faults during earthquake slip. J. Geophys. Res, 111, B05311

Rice JR., 1992. Fault stress states, pore pressure distributions, and the weakness of the San Andreas Fault. In Fault Mechanics and Transport Properties of Rocks, ed. B Evans, Tf Wong, pp. 475–504. London: Academic.

Segall, P. & Rice, J.R., 2006. Does shear heating of pore fluid contribute to earthquake nucleation? J. geophys. Res., 111, B09316

Sibson R.H., 1973. Interactions between Temperature and Pore-Fluid Pressure during Earthquake Faulting and a Mechanism for Partial or Total Stress Relief, Nature, 243, 66–68

Smith S.A.F. Nielsen S., Di Toro G. 2015. Strain localization and the onset of dynamic weakening in calcite fault gouge. Earth Planet. Sci. Lett., 413, 25-36

Tsutsumi A., Shimamoto T., 1997. High-velocity frictional properties of gabbro. Geophys. Res. Lett., 24, 699–702

Ujiie K., Tsutsumi A., Kameda J.2011. Reproduction of thermal pressurization and fluidization of clay-rich fault gouges by high-velocity friction experiments and implications for seismic slip in natural faults Rick Sibson, Geological Society of London Special Publication, 359, 267–285

Ujiie, K., *et al.* 2013, Low coseismic shear stress on the Tohoku-oki megathrust determined from laboratory experiments, Science, 342, 1211–1214.

Verberne B.A, et al., 2014. Superplasticnanofibrous slip zones control seismogenicfault friction Science. 346, 1342-1344.

Vinciguerra S., et al., 2005. Relating seismic velocities, thermal cracking and permeability in Mt. Etna and Iceland basalts J. Rock Mech., 42900-42910.

Violay M. et al., 2012. Pore fluid in experimental calcite-bearing faults: abrupt weakening and geochemical signature of co-seismic processes. Earth Planet. Sci. Lett. 361, 74–84

Violay M. et al., 2014. Effect of glass on the frictional behavior of basalts at seismic slip rates, Geophys. Res. Lett. 41, 348-355

Violay M. et al., 2014. Effect of water on the frictional behavior of cohesive rocks during earthquakes. Geology. 42, 27-30

Waples, D.W., Waples, J.S., 2004. A review and evaluation of specific heat capacities of rocks, minerals, and subsurface fluids. Part 1: Minerals and nonporous rocks. Nat. Resour. Res. 13 , 13–130.

Wibberley, C.A.J. Shimamoto T, 2005. Earthquake slip weakening and asperities explained by thermal pressurization. Nature, 436, 689–692.

ACKNOWLEDGMENTS

We thank R. Lüchinger (ETH) for thin sections preparation and P. Scarlato (INGV), and E. Reusser (ETH) for laboratory support. We acknowledge S. Vinciguerra and R. Bakker for their help with the experiments. MV and JPB thank the ETH and GDT, SN and ES the ERC grant No 614705 NOFEAR for the financial support.

FIGURES:

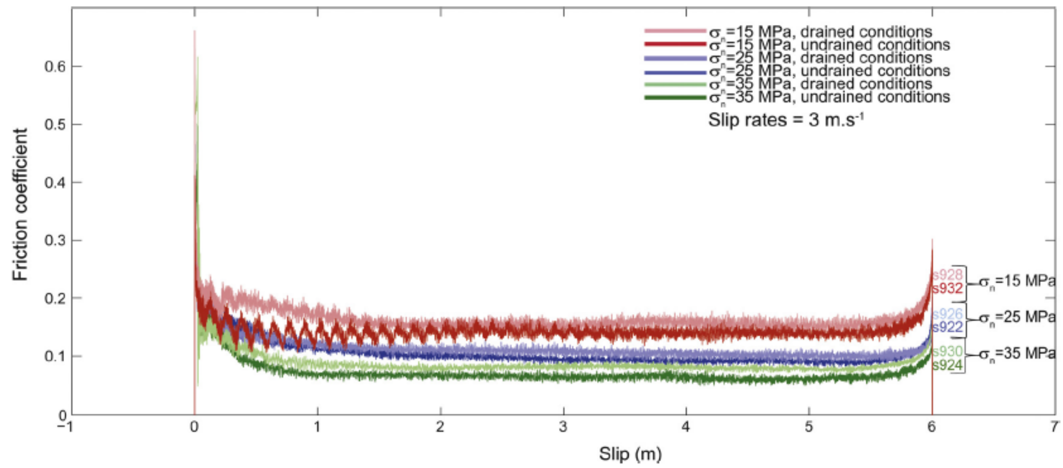

Figure. 1: Friction coefficient versus slip in Etna basalt. Experiments were performed at slip rate, $V = 3$ ms^{-1} (target slip rate), acceleration = 7.8 ms^{-2}, and initial σ_n^{eff} comprised between 10 MPa and 30 MPa under either drained conditions (experiments s928, s926 and s930), and undrained conditions (s932, s922, and s924). Independently of the initial σ_n^{eff}, a reduction of ~20% of μ_{ss} was measured in the experiments performed under undrained conditions.

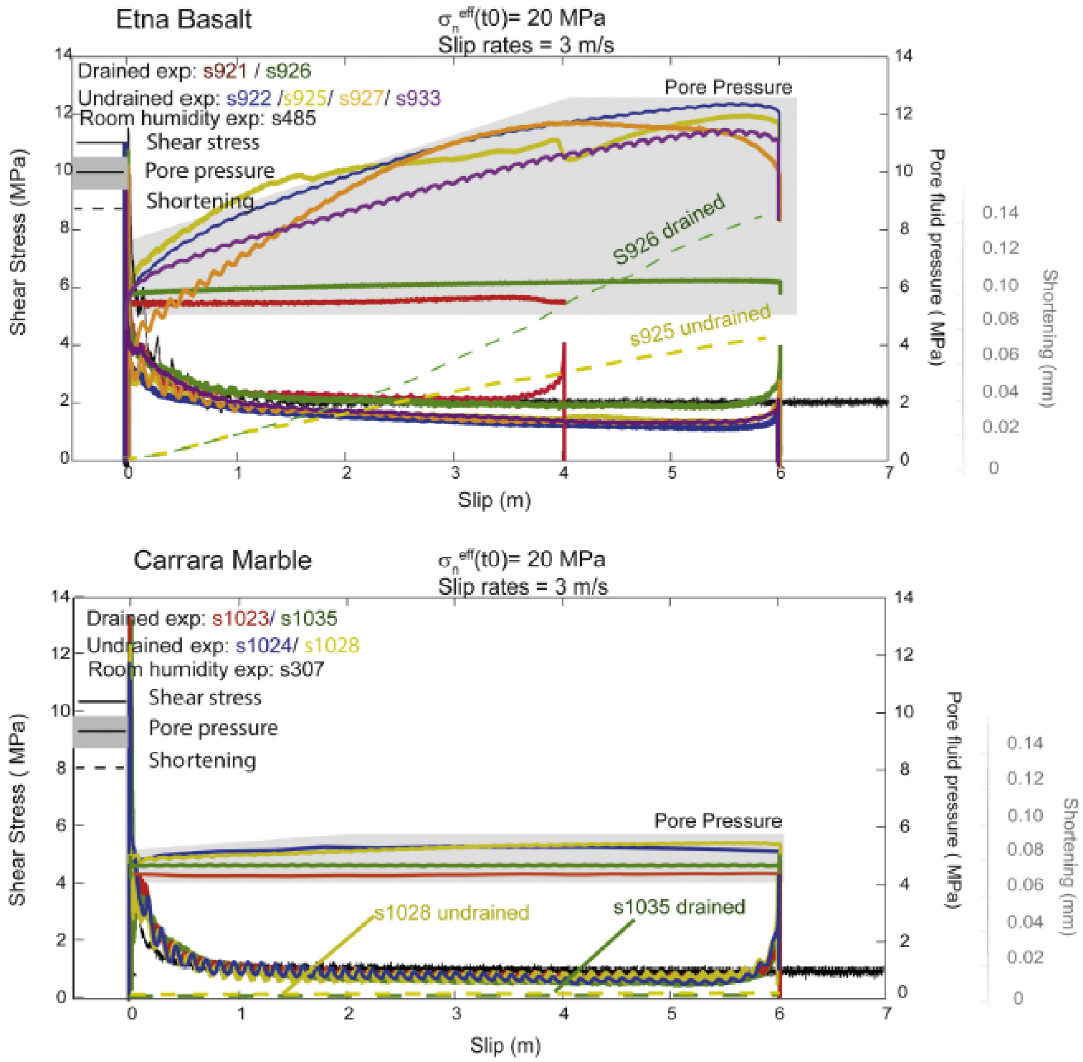

Figure 2: Shear stress versus slip in Etna basalt and Carrara marble. Experiments were performed at V = 3 ms^{-1} (target slip rate), acceleration = 7.8 ms^{-2}, and $\sigma_n{}^{eff}$= 20 MPa at the initiation of the experiments under following environmental and hydraulic conditions: A) Etna basalt: room-humidity (s485σ_n= 20 MPa: black curve), pore water under drained conditions (s921 and s926: red and green curve), pore water under undrained conditions (s922, s925, s927 and s933: yellow, orange, purple, and blue curves).B) Carrara marble: room-humidity (s307 σ_n= 20 MPa: black curve), pore water under drained conditions (s1023 and s1035: red and green curve), pore water under undrained conditions (s1024 and s1028: yellow and blue curves). Pore water pressure (full line) and shortening (dashed line)for drained andundrained experiments are depicted with the same colors as the reported shear stress.

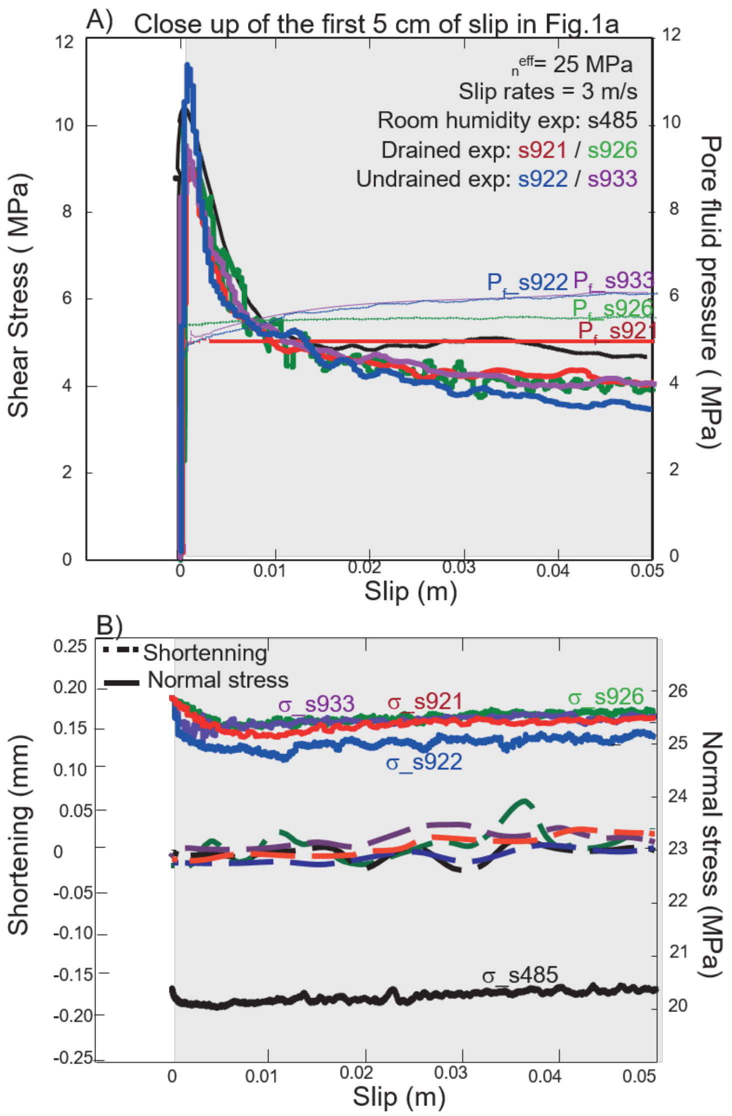

Figure 3: Mechanical data. A) Close up of the first 0.05 m of slip of Fig. 1A for experiments s485 (room-humidity, black curve), s922, s933 (drained, purple and blue curves), s921, s926, (undrained, red and green curves). Pore water pressure for drained andundrained experiments are depicted with the same colors as the reported shear stress. B) Normal effective stress and shortening versus slip plot for experiments s485 (room-humidity, black curve), s922, s933 (drained, purple and blue curves), s921 and s926 (undrained, red and green curves).

Fig.3

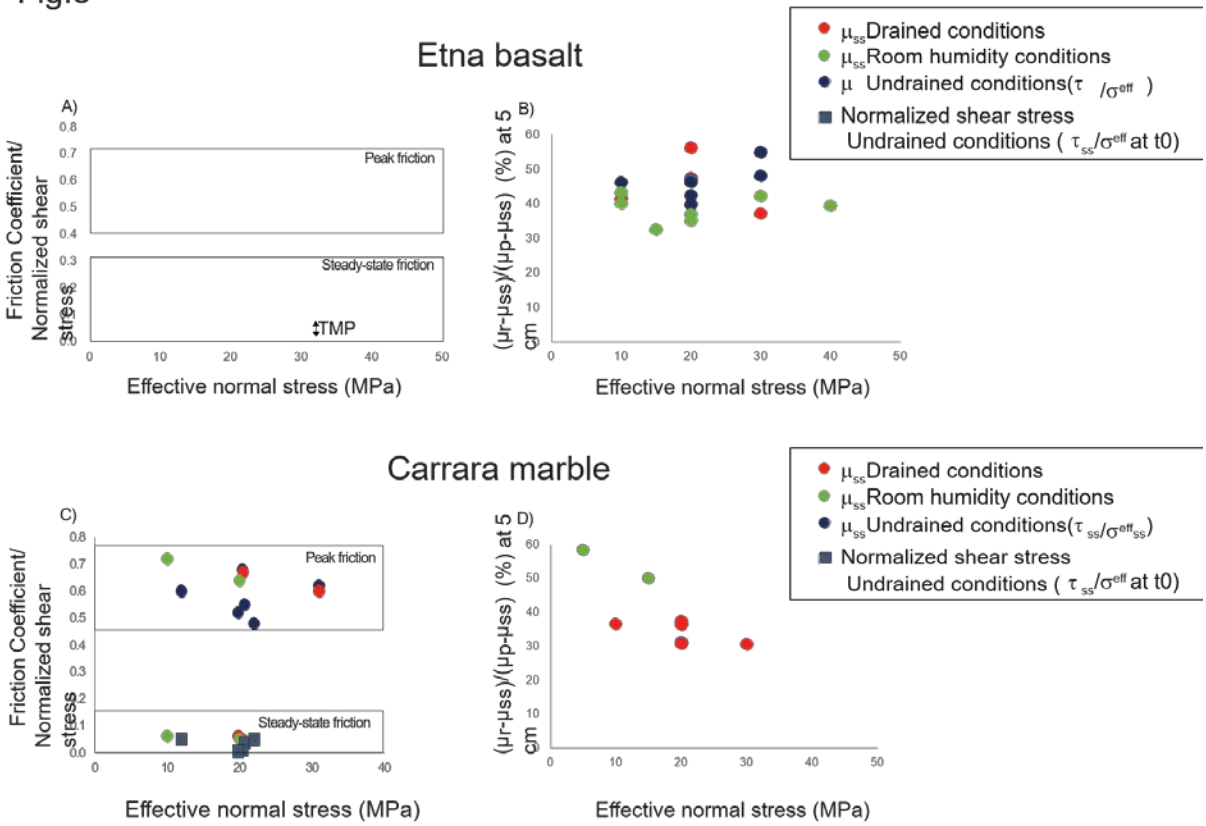

Figure 4: Summary figure of the mechanical data for Etna basalt(22 experiments, Figs. A and B) and Carrara marble (11 experiments, Figs. C and D) reported in this study. Experiments were performed at V = 3 ms^{-1} (target slip rate), acceleration = 7.8 ms^{-2}, and P_f ~5 MPa at the initiation of the drained and undrained experiments. A) Etna basalt: - friction coefficient vs. effective normal stress effective with respect to the pore fluid pressureat steady-state($\sigma_n^{eff}=\sigma_n$ –(P_{ini} + $P_{TMP}(t)$), i.e total fluid pressure, including variations due to fluid heating and mechanical effects of sample shortening and volume change in the vessel) under room-humidity conditions (green circles), drained conditions (red circles) and undrained conditions. - Blue squares: Friction coefficient vs. effective normal stress with respect to the pore fluid pressure at the initiation of the experiment ($\sigma_n^{eff}=\sigma_n$ -P_{ini}). B) Etna basalts: percentage of residual friction with respect to the steady-state friction after 5 cm of slip vs. effective normal stress under room-humidity conditions (green circles) drained conditions (red circles) and undrained conditions (blue circles). Y axis: μ_p= peak friction, μ_{ss} = steady-state friction, μ_r = residual friction. (C) and (D), case for Carrara Marble. Standard deviation is within the dimension of the symbols.

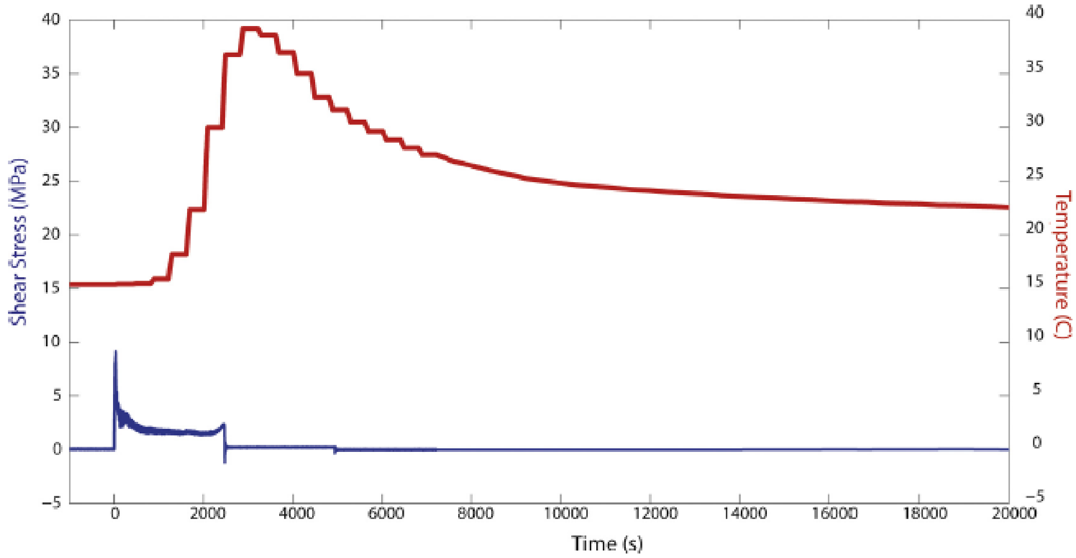

Figure 5: Evolution of the shear stress (blue curve) and temperature (red curve) measured by the thermocouple during experiment s929 (undrained conditions).

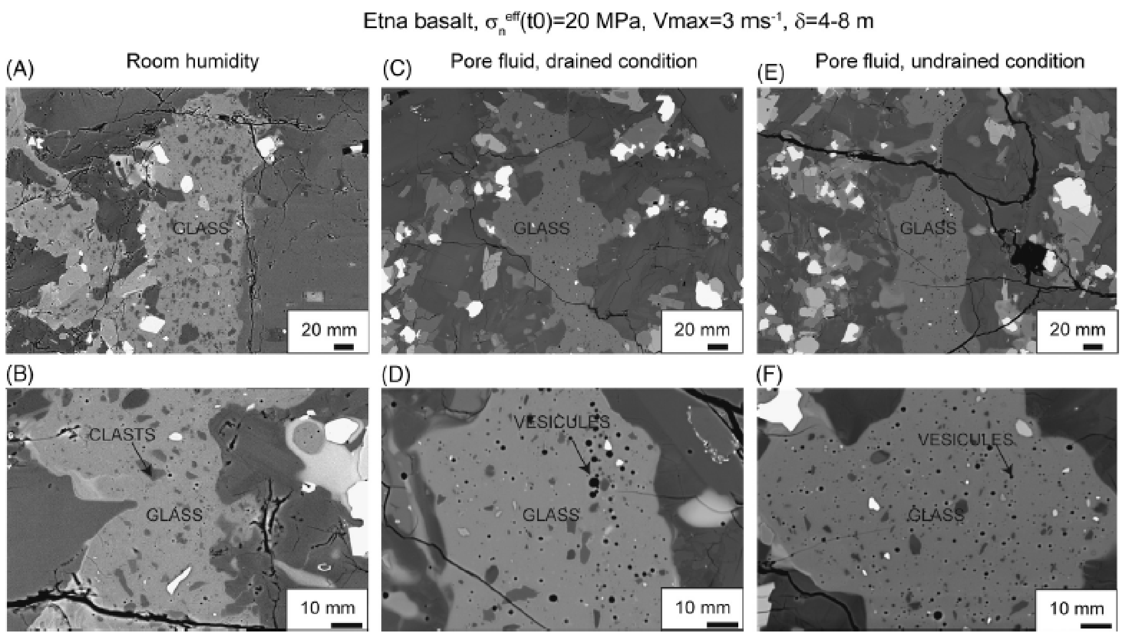

Figure 6: Slipping zones of Etna basalt after steady-state friction was achieved (>1 m of slip). Experimental conditions: acceleration 7.8 ms^{-2}, initial $\sigma_n{}^{eff}$= 20 MPa and slip rate, V = 3 ms^{-1}. A-B: Room-humidity conditions C-D: Drained conditions. E-F:Undrained conditions.Independentlyof the environmental conditions, at the end of experiments, the wall

rocks were separated by continuous layer of glass. B, D and Fare enlargements of the slipping zones. Field emission scanning electron microscope- Backscattered electronimages.

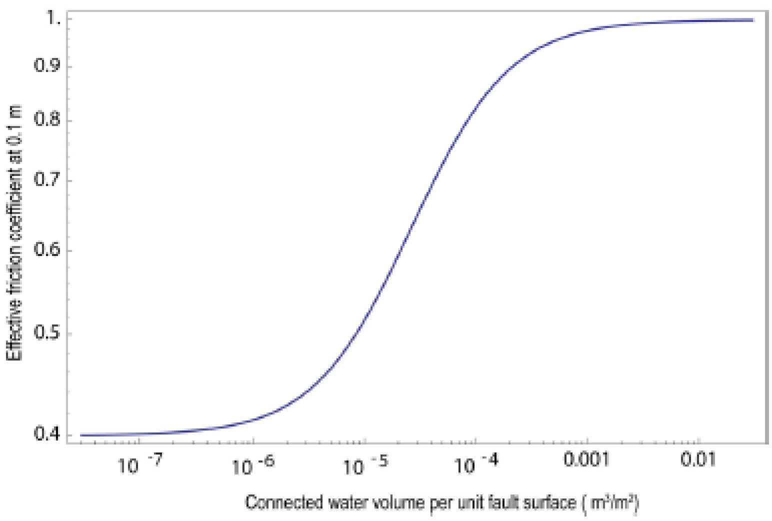

Figure 7: Weakening due to water pressurization w_p versus the connected volume per unit fault surface (values of $w_p = 1$ correspond to no weakening). Maximum effect of pressurization is a drop to 40% for connected volumes of less than a cubic centimeter per unit fault area. For values above 1 liter of connected buffering water, the pressurization effect is negligible.

Experiment #	Lithology	Conditions	Target slip rate ($m s^{-1}$)	Normal stress (MPa)	Initial pore fluid pressure (MPa)	Initial normal effective stress (MPa)	Peak friction coefficient for initial pore pressure ±0.08	Steady-state friction coefficient for pore pressure at steady-state ±0.02	Friction coefficient at 5 cm of slip for pore pressure at 5 cm slip	% drop friction coefficient after 5 cm of slip	Steady-state shortening rate (mm/m)
s928	E.B.	drained	3.0	15.0	4.4	10.6	0.63	0.16	0.26	78.7	0.123
s921	E.B.	drained	3.0	25.0	5.3	19.7	0.50	0.11	0.28	56.4	0.145
s926	E.B.	drained	3.0	25.0	5.4	19.6	0.55	0.10	0.26	64.4	0.123
s930	E.B.	drained	3.0	35.0	5.3	29.7	0.62	0.08	0.23	72.2	0.280
s929	E.B.	undrained	3.0	15.0	4.7	10.3	0.49	0.13	0.23	72.2	0.018
s922	E.B.	undrained	3.0	25.0	4.6	20.4	0.58	0.09	0.23	71.4	0.098
s925	E.B.	undrained	3.0	25.0	4.9	20.1	0.50	0.10	0.23	67.5	0.065
s927	E.B.	undrained	3.0	25.0	4.5	20.5	0.52	0.10	0.22	71.4	0.083
s933	E.B.	undrained	3.0	25.0	4.9	20.1	0.50	0.10	0.24	65.0	0.065
s923	E.B.	undrained	3.0	35.0	4.4	30.6	0.52	0.06	0.24	60.9	0.125
s932	E.B.	undrained	3.0	15.0	5.2	9.8	0.42	0.14	0.23	67.9	0.038
s924	E.B.	undrained	3.0	35.0	4.8	30.2	0.68	0.07	0.25	70.5	0.275
s486	E.B.	room humidity	3.0	5.0	0.0	5.0	0.69	0.28			0.040
s484	E.B.	room humidity	3.0	10.0	0.0	10.0	0.57	0.17			
s652	E.B.	room humidity	3.0	10.0	0.0	10.0	0.65	0.17	0.28	77.1	0.128
s542	E.B.	room humidity	3.0	10.0	0.0	10.0	0.70	0.10	0.28	70.0	0.055
s651	E.B.	room humidity	3.0	15.0	0.0	15.0	0.68	0.08	0.22	76.3	0.305
s485	E.B.	room humidity	3.0	20.0	0.0	20.0	0.57	0.11	0.20	80.2	0.240
s541	E.B.	room humidity	3.0	20.0	0.0	20.0	0.68	0.11	0.25	75.4	0.200
s697	E.B.	room humidity	3.0	25.0	0.0	25.0	0.55	0.03			
s543	E.B.	room humidity	3.0	30.0	0.0	30.0	0.69	0.07	0.21	77.7	0.293
s487	E.B.	room humidity	3.0	40.0	0.0	40.0	0.61	0.06	0.24	67.6	
s1033	C.M.	undrained	3.0	15.0	3.0	12.0	0.60	0.06	0.22	70.4	0.000
s1028	C.M.	undrained	3.0	25.0	4.3	20.7	0.55	0.04	0.20	68.6	0.000
s1029	C.M.	undrained	3.0	25.0	3.0	22.0	0.48	0.04	0.18	68.2	−0.006
s1030	C.M.	undrained	3.0	25.0	4.6	20.4	0.68	0.02	0.21	71.2	0.000
s1031	C.M.	undrained	3.0	25.0	5.2	19.8	0.52	0.00	0.16	69.5	0.003
s1024	C.M.	undrained	3.0	25.0	4.7	20.3	0.50	0.04	0.20	65.2	0.001
s1034	C.M.	undrained	3.0	35.0	4.0	31.0	0.62	0.00	0.19	69.6	
s1023	C.M.	drained	3.0	25.0	4.5	20.5	0.60	0.04	0.22	67.9	−0.001
s1035	C.M.	drained	3.0	25.0	5.2	19.9	0.67	0.04	0.21	73.0	0.000
s330	C.M.	room humidity	3.0	10.0	0.0	10.0	0.72	0.06	0.42	45.5	0.000
s307	C.M.	room humidity	3.0	20.0	0.0	20.0	0.64	0.05	0.32	54.2	0.000

Table 1: Summary of experimental conditions and results. See main text for explanations. C.M. = Carrara marble; E.B.=Etna basalt.

Sample phase #	Etna basalt Crystalline*	s485 dry glass 15	S.D.	s921 drained glass 15	S.D.	s925 undrained glass 15	S.D.
SiO_2	47.03	49.09	0.94	48.41	0.37	48.17	0.46
Na_2O	3.75	4.20	0.13	3.24	0.21	3.44	0.10
CaO	10.47	10.13	0.23	9.64	0.20	9.70	0.10
K_2O	1.94	1.84	0.13	1.67	0.10	1.70	0.03
FeO	10.80	8.34	0.33	8.77	0.32	9.21	0.07
Al_2O_3	16.28	19.41	0.30	18.64	0.39	17.51	0.21
MgO	5.17	3.88	0.19	4.46	0.15	5.17	0.06
TiO_2	1.61	1.45	0.16	1.55	0.06	1.57	0.04
P_2O_5	0.59	0.65	0.01	0.55	0.04	0.55	0.03
MnO	0.20	0.16	0.07	0.18	0.01	0.17	0.02
Total	97.84	99.46	0.97	97.11	0.46	97.20	0.67

* Giordano and Dingwell (2003).

Table 2: Chemical composition of the basalt and of the glass. Chemical bulk composition of the Etna basalt (Giordano and Dingwell, 2003*); Electron MicroProbe Analysis (EMPA) chemical compositions ofthe initial glass and of the solidified frictional melt. The EPMA analysis do not close to about 100% because only Fe2+ was determined. The S.D. refers to the standard deviation of the EMPA composition of the solidified friction melts.

* Giordano and Dingwell. 2003. Viscosity of hydrous Etna basalt: implications for plinian-style basaltic eruptions. bullVolcanol 65:8-14.